# Antibunching of distorted optical wave packets at a beam splitter

Toralf Gruner [1] and Dirk–Gunnar Welsch

*Theoretisch-Physikalisches Institut, Friedrich-Schiller-Universität Jena*
*D-07743 Jena, Germany*

Interference of single-photon wave packets at a beam splitter usually leads to an anticorrelation of the light intensity in the two output ports of the beam splitter. The effect may be regarded as "bunching" of the photons at the beam splitter and has widely been interpreted as a result of quantum mechanical interference between the probability amplitudes of indistinguishable bosonic particles. Here we show that when the wave packets are sufficiently distorted, then the opposite behaviour is observed, i.e., simultaneous clicks of the photodetectors in the two output ports are favoured, which may be regarded as "antibunching" of the photons at the beam splitter.

PACS number(s): 42.25.Hz, 42.50.Ct, 42.25.Bs, 42.30.Lr

Keywords: radiation-field quantization, input-output relations, multilayer dielectric systems, photonic bandgaps, photon tunneling

## 1 Introduction

The study of the interference behaviour of quantized light has not only been of fundamental interest, but has also been important for applications, such as the use of nonclassical light in highly sensitive interferometry. In particular, two-photon interference experiments have offered new possibilities of studying fourth-order interference phenomena of single-photon wave packets [1–5]. An interesting phenomenon is the anticorrelation of the photoelectric counts recorded in the two output channels of a beam splitter [6] or an optical fibre multiport [7]. The dependence of the coincidence events on the optical delay

[1] Present address: Carl Zeiss, Optical Design Dept., D-73446 Oberkochen, Germany

between the two interfering wave packets can be used to determine the photon tunneling time through an optical barrier [8–10].

In order to explain the anticorrelation (bunching) behaviour of interfering single-photon wave packets in the output channels of a beam splitter, it has been argued that when two photons arrive at the beam splitter simultaneously, then the outgoing state is obtained by superposition of probability amplitudes, because of the indistinguishability of the photons. Such an interpretation could imply the conclusion that the interference phenomenon observed is a pure quantum effect. On the other hand it has been shown that the effect also appears for independent classical light fields [11]. It may therefore be expected that classical and nonclassical light fields give rise to quantitatively rather than qualitatively different interference structures of the coincidence-event statistics. In this context, the question arises of what is the effect on the interference fringes of correlated incoming beams and whether or not the interference fringes enable one to distinguish between classical and nonclassical light.

In this paper we show that when single-photon wave packets whose superposition gives rise to anticorrelations in the coincidence-event statistics in the two output ports of a beam splitter are sufficiently strong distorted by a multilayer dielectric slab and a superposition of the distorted wave packets is measured, then correlations can be observed in place of anticorrelations. Such a behaviour may be regarded as a kind of "antibunching", which would be expected for fermionic particles rather than photons. Clearly, identifying the distorted wave packets with single photons can be quite questionable, as has been stressed recently [10]. Moreover, correlations can only be observed when the two incoming wave packets are produced by the same source and the overall field is in a correlated state. We analyse possible interference structures and discuss criteria for deciding from the observed interference fringes whether the incoming fields are classical or not and whether they are correlated or independent of each other.

The paper is organized as follows. In Sec. 2 the underlying formalism for describing the propagation of quantized light through multilayer dielectric structures is outlined. In Sec. 3 a Mach–Zehnder interferometer is considered and the interference fringes of the output coincidence events are determined in dependence on the distortion of the beams in the two arms. Finally, a summary is given in Sec. 4.

## 2 Field quantization and input-output relations

To describe the interaction of quantized radiation with (linearly responding) dielectric matter, we use the quantization scheme developed in [12–14], which is based on the determination of the Green function of the classical propagation problem. In particular, we consider linearly polarized light propagating in $x$ direction through a dielectric plate consisting of $N = M - 2$ layers ($M \geq 3$). The operator of the vector potential can then be given by [14]

$$\hat{A}(x) = \sum_{j=1}^{M} \lambda_j(x) \int_0^\infty \mathrm{d}\omega \sqrt{\frac{\hbar \beta_j(\omega)}{4\pi c \omega \epsilon_0 \epsilon_j(\omega) \mathcal{A}}} \times \left[ e^{i\beta_j(\omega)\omega x/c}\, \hat{a}_{j+}(x,\omega) + e^{-i\beta_j(\omega)\omega x/c}\, \hat{a}_{j-}(x,\omega) \right] + \text{H.c.}, \tag{1}$$

where $\lambda_j(x) = 1$ if $x_{j-1} < x < x_j$ and $\lambda_j(x) = 0$ otherwise, $\epsilon_j(\omega) = n_j^2(\omega)$ with $n_j(\omega) = \beta_j(\omega) + i\gamma_j(\omega)$ is the complex permittivity of the $j$th layer, and $\mathcal{A}$ is the normalization area in the $yz$ plane [$j = 1$ and $j = M$ refer to the left- and right-hand side free-space surroundings of the plate, respectively, with $\epsilon_1(\omega) = \epsilon_M(\omega) = 1$]. The quasi-mode operators $\hat{a}_{j\pm}(x,\omega)$ inside the plate are associated with (damped) waves propagating to the right and left, respectively. Outside the plate they are independent of $x$ and obey the familiar bosonic commutation relations for photons in free space,

$$\left[ \hat{a}_{1\pm}(\omega), \hat{a}_{1\pm}^\dagger(\omega') \right] = \delta(\omega - \omega'), \tag{2}$$

$$\left[ \hat{a}_{M\pm}(\omega), \hat{a}_{M\pm}^\dagger(\omega') \right] = \delta(\omega - \omega'), \tag{3}$$

$$\left[ \hat{a}_{1\pm}(\omega), \hat{a}_{M\mp}^\dagger(\omega') \right] = 0, \tag{4}$$

where the output operators $\hat{a}_{1-}(\omega)$, $\hat{a}_{M+}(\omega)$ are related to the input operators $\hat{a}_{1+}(\omega)$, $\hat{a}_{M-}(\omega)$ and bosonic operators of the plate excitations, $\hat{g}_\pm(\omega)$, as

$$\begin{pmatrix} \hat{a}_{1-}(\omega) \\ \hat{a}_{M+}(\omega) \end{pmatrix} = \tilde{\mathbf{T}}(\omega) \begin{pmatrix} \hat{a}_{1+}(\omega) \\ \hat{a}_{M-}(\omega) \end{pmatrix} + \tilde{\mathbf{A}}(\omega) \begin{pmatrix} \hat{g}_+(\omega) \\ \hat{g}_-(\omega) \end{pmatrix}, \tag{5}$$

$$\left[ \hat{g}_\pm(\omega), \hat{g}_\pm^\dagger(\omega') \right] = \delta(\omega - \omega'). \tag{6}$$

In Eq. (5), $\tilde{\mathbf{T}}$ and $\tilde{\mathbf{A}}$, respectively, are the characteristic transformation and absorption matrices of the multilayer plate [14]. Note, that the elements of $\tilde{\mathbf{T}}$ and $\tilde{\mathbf{A}}$ are not independent of each other, but they are related to each other such that the consistency of the quantization scheme is ensured.

## 3 Fourth-order interference

Let us consider an experimental scheme of the type studied in [8] (Fig. 1). Pairs of correlated (single-photon) wave packets produced in a parametric down conversion process are combined by a lossless 50%:50% beam splitter (BS) and the time-integrated output coincidences

$$R(s) = \xi^2 \int \mathrm{d}t_1 \int \mathrm{d}t_2 \left\langle \hat{E}^{(-)}(t_1)\hat{E}^{(-)}(t_2)\hat{E}^{(+)}(t_1)\hat{E}^{(+)}(t_2)\right\rangle \tag{7}$$

are measured (the detectors $\mathrm{PD}_1$ and $\mathrm{PD}_2$ in Fig. 1 are assumed to have equal efficiency $\xi$). In contrast to [8], here each of the two wave packets is allowed to pass a dielectric barrier (DB 1 and DB 2 in Fig. 1) before impinging on the beam splitter. The position of a prism (P) in one arm of the interferometer is adjusted such that the additional path (2s) compensates for the difference between the propagations of the two wave packets trough different barriers.

To calculate $R(s)$, Eq. (7), we first relate the fields $\hat{E}^{\pm}(t_1)$ and $\hat{E}^{\pm}(t_2)$ at the two detectors to the fields produced by the source, applying the input–output relations (5) and assuming that the barriers are in the ground state (zero-temperature limit). In a quantum-mechanical description we then perform the averaging $\langle\cdots\rangle$ in Eq. (7) assuming that the down-conversion photons are initially prepared in an entangled state

$$|\Psi\rangle = \int_0^\infty \mathrm{d}\Omega\, \alpha(\Omega) \int_0^\Omega \mathrm{d}\omega\, f(\omega) f(\Omega-\omega)\, \hat{a}_{\mathrm{I}}^\dagger(\omega)\, \hat{a}_{\mathrm{II}}^\dagger(\Omega-\omega)\, |0\rangle, \tag{8}$$

where the subscripts I and II refer to the two arms of the interferometer (see Fig. 1), and $\alpha(\Omega)$ and $f(\omega)$, respectively, denote the band-shape functions of the laser and the down-conversion photons, $f(\omega)$ being centered at $\Omega/2$. After some calculation we derive

$$R(s) = 2\pi^2 \mathcal{N}^4 \xi^2 \left[K_0 - K_1(s)\right], \tag{9}$$

$\mathcal{N} = \sqrt{\hbar/(4\pi c\epsilon\mathcal{A})}$, where

$$K_0 = \int_0^\infty \mathrm{d}\Omega\, \alpha^2(\Omega) \int_0^\Omega \mathrm{d}\omega\, \omega(\Omega-\omega) \left| T_{21}^{(\mathrm{I})}(\omega) f(\omega) T_{21}^{(\mathrm{II})}(\Omega-\omega) f(\Omega-\omega)\right|^2 \tag{10}$$

is independent of the position of the prism, $s$, and the position-dependent part $K_1(s)$ reads as

$$K_1(s) = \int_0^\infty \mathrm{d}\Omega\, \alpha^2(\Omega) \int_0^\Omega \mathrm{d}\omega\, \omega(\Omega-\omega)\, |f(\omega) f(\Omega-\omega)|^2 \times e^{2i(2\omega-\Omega)s/c} T_{21}^{(\mathrm{I})^*}(\omega) T_{21}^{(\mathrm{I})}(\Omega-\omega) T_{21}^{(\mathrm{II})^*}(\Omega-\omega) T_{21}^{(\mathrm{II})}(\omega). \tag{11}$$

In Eqs. (10) and (11), $T_{ij}^{(\mathrm{I/II})}$ $(i,j=1,2)$ are the elements of the characteristic transformation matrices $\tilde{\mathbf{T}}^{(\mathrm{I/II})}$ of the two dielectric barriers (for analytical results for lossless and lossy Bragg mirrors, respectively, see [15] and [14]).

Let us compare this result with that obtained when a classical light source is considered which in a complete random way produces correlated pairs of wave packets. Straightforward calculation yields [16]

$$R(s) = 4\pi^2 \xi^2 \left[ G_0 - G_1(s) \right], \tag{12}$$

where

$$G_0 = \left\langle \int_0^\infty \mathrm{d}\omega \int_0^\infty \mathrm{d}\omega' \left[ 2 \left| T_{21}^{(\mathrm{I})}(\omega) E^{(\mathrm{I})}(\omega) \right|^2 \left| T_{21}^{(\mathrm{II})}(\omega') E^{(\mathrm{II})}(\omega') \right|^2 + \left| T_{21}^{(\mathrm{I})}(\omega) E^{(\mathrm{I})}(\omega) T_{21}^{(\mathrm{I})}(\omega') E^{(\mathrm{I})}(\omega') \right|^2 + \left| T_{21}^{(\mathrm{II})}(\omega) E^{(\mathrm{II})}(\omega) T_{21}^{(\mathrm{II})}(\omega') E^{(\mathrm{II})}(\omega') \right|^2 \right] \right\rangle_{\mathrm{cl}} \tag{13}$$

and

$$G_1(s) = 2\mathrm{Re}\left\{ \left\langle \int_0^\infty \mathrm{d}\omega \int_0^\infty \mathrm{d}\omega' e^{2i(\omega-\omega')s/c}\, T_{21}^{(\mathrm{I})}(\omega') E^{(\mathrm{I})}(\omega') T_{21}^{(\mathrm{II})}(\omega) E^{(\mathrm{II})}(\omega) \times \left[ T_{21}^{(\mathrm{I})}(\omega) E^{(\mathrm{I})}(\omega) T_{21}^{(\mathrm{II})}(\omega') E^{(\mathrm{II})}(\omega') \right]^* \right\rangle_{\mathrm{cl}} \right\}. \tag{14}$$

Here, $\langle \cdots \rangle_{\mathrm{cl}}$ denotes a classical averaging, the complex-valued Fourier components of the emitted (down-conversion) fields in the two arms of the interferometer, $E^{(\mathrm{I})}(\omega)$ and $E^{(\mathrm{II})}(\omega)$, being the random variables. Note that from Eqs. (13) and (14) the relation

$$\frac{|G_1(s)|}{G_0} \leq \tfrac{1}{2} \tag{15}$$

can be derived [16].

To perform the classical averaging, the (joint) probability distributions for $E^{(\mathrm{I})}(\omega)$ and $E^{(\mathrm{II})}(\omega)$ must be specified. To compare the quantum regime as

given by the state in Eq. (8) with a classical regime that is as similar as possible to the quantum regime, we assume that the probability distributions are such that the frequencies and phases of the laser fields and the down-conversion fields are related to each other as $\delta(\Omega-\omega-\omega')$ and $\delta(\varphi_{\rm L}-\varphi_{\rm I}-\varphi_{\rm II})$ ($\varphi_{\rm L}$ is the laser phase and $\varphi_{\rm I}$, $\varphi_{\rm II}$ are the phases of the two down-conversion fields). In the spirit of close correspondence between classical and quantum regime we then may assume that Eqs. (13) and (14) can be rewritten as

$$\begin{aligned} G_0 = 2\int\limits_0^\infty {\rm d}\omega\,\omega(\Omega-\omega)\left|T_{21}^{({\rm I})}(\omega)f(\omega)T_{21}^{({\rm II})}(\Omega-\omega)f(\Omega-\omega)\right|^2 \\ + \int\limits_0^\infty {\rm d}\omega\,\omega(\Omega-\omega)\left|T_{21}^{({\rm I})}(\omega)f(\omega)T_{21}^{({\rm I})}(\Omega-\omega)f(\Omega-\omega)\right|^2 \\ + \int\limits_0^\infty {\rm d}\omega\,\omega(\Omega-\omega)\left|T_{21}^{({\rm II})}(\omega)f(\omega)T_{21}^{({\rm II})}(\Omega-\omega)f(\Omega-\omega)\right|^2 \end{aligned} \tag{16}$$

and

$$\begin{aligned} G_1(s) = 2\int\limits_0^\infty {\rm d}\omega\,\omega(\Omega-\omega)\left|f(\omega)f(\Omega-\omega)\right|^2 \\ \times e^{2i(2\omega-\Omega)s/c}T_{21}^{({\rm I})^*}(\omega)T_{21}^{({\rm I})}(\Omega-\omega)T_{21}^{({\rm II})^*}(\Omega-\omega)T_{21}^{({\rm II})}(\omega), \end{aligned} \tag{17}$$

where $f(\omega)$ is the same band-shape function as in Eq. (8).

The classical relations (16) and (17) and the quantum-mechanical relations (10) and (11) are seen to mainly differ in the second and third terms in Eq. (16). Physically, these terms are related to coincidence events caused either by the field in the arm I or the field in the arm II, since a classical field in one arm of the interferometer can always be decomposed into two parts by means of the beam splitter. The corresponding coincidence events are of course independent of the prism position $s$ and hence the fringe visibility

$$\mathcal{V} = \frac{R_{\rm max}-R_{\rm min}}{R_{\rm max}+R_{\rm min}} \tag{18}$$

diminishes. Clearly, in the quantum regime a single photon in one of the arms cannot give rise to a coincidence event.

Let us first assume that the barriers in the arms of the interferometer are absent and the prism is translated such that the two wave packets do not overlap at the beam splitter, i.e., $s\to\infty$. As expected, there is no $s$-dependent interference effect, because the interference terms in Eqs. (9) and (12) vanish,

i.e., $G_1(s) \to 0$ and $K_1(s) \to 0$, as it can easily be seen from Eqs. (11) and (17), respectively. In the quantum regime single-photon wave packets impinge separately on the beam splitter, where they are either reflected or transmitted with 50% probability in each case. In the classical regime the incident wave packets correspond, in a sense, to multiphoton states, because there is no classical analogue of a single-photon state. Hence, a wave packet that impinges on the beam splitter is split into two parts of equal intensity, which implies that coincidence events are preferably observed [see the second and third term in Eq. (16) – terms that are not observed in Eq. (10)].

To study the interference behaviour, let us introduce the normalized time-integrated coincidence events $R^{(\mathrm{n})}(s) = R(s)/R(\infty) = [K_0 - K_1(s)] \,/\, K_0$ [or $= [G_0 - G_1(s)] \,/\, G_0$ in the classical regime]. From Fig. 2 it can be seen that in the quantum regime $R^{(\mathrm{n})}(s)$ decreases with decreasing value of $s$ (compared to $s \to \infty$) and attains a zero-value minimum. This behaviour can be explained from the argument of the indistinguishability of the two (now interfering) photons – there is no "which-way"-information available at the detectors, because of the wave combination at the beam splitter. The minimum is observed for equal optical lengths of the two paths I and II through the interferometer (i.e., $s = 0$ in the figure). It should be pointed out that a qualitatively similar behaviour is also observed in the classical regime, which can be explained using standard arguments of classical optics. The difference between the quantum and classical regime is that in the latter the fringe visibility is substantially reduced. Recalling Eq. (15), it is easily seen that – compared to the zero-value minimum in the quantum regime – in the classical case $R^{(\mathrm{n})}(0) = 1/2$ is valid.

Let us now consider the case when a Bragg mirror is introduced in one arm of the interferometer (say, the second arm). In Fig. 3 the dependence on frequency of the square of the absolute value of the transmittance of an assumed barrier, $|T_{21}(\omega)|^2$, and the absolute value of the band-shape function of an assumed time-limited wave packet, $|f(\omega)|$, are plotted, $|f(\omega)|$ being centered at the middle of the band gap (2.68 PHz). Note that in the Berkeley experiments [8] the number of layers the barrier is composed of is $N = 11$. Examples of $R^{(\mathrm{n})}(s)$ for the quantum regime are shown in Fig. 4 and discussed in detail in Ref. [10]. Here it should be pointed out that when $N$ is not too large (e.g., $N = 11$ in Fig. 4) $R^{(\mathrm{n})}$ is always smaller then unity, whereas for sufficiently large $N$ (e.g., $N = 41$ in Fig. 4) it becomes also possible that $R^{(\mathrm{n})} > 1$. Clearly, such a behaviour cannot be explained from interference of probability amplitudes of indistinguishable quanta, but this is not very surprising if we recall the strong distortion of a wave packet at such a barrier [10].

Since with increasing number of layers, $N$, the transmittance of the barrier drastically decreases, it may be difficult to observe the effect in the scheme considered so far. However, it may easily be observed if the laser is detuned such that the band-shape function $f(\omega)$ bridges over a band-gap edge of the

barrier and sufficiently overlaps a region of (fractional) transparency. From the interference fringes shown for the quantum regime in Fig. 5, in which $|f(\omega)|$ is assumed to be centered at the upper band-gap edge (3.06 PHz), it is clearly seen that the number of coincidence events can be reduced ($R^{(\mathrm{n})}<1$) as well as enhanced ($R^{(\mathrm{n})}>1$). Note that with decreasing $N$ the main minimum survives, whose position at $s<0$ indicates subliminal behaviour.

It could be thought that the effect of enhanced coincidences results from the distortion of the wave packet at the barrier relative to the undisturbed wave packet in the other arm of the interferometer. That this is not the case can be seen from Fig. 6 (for the quantum regime). In the figure it is assumed that the two wave packets are distorted in the same way, introducing identical Bragg mirrors in the two arms of the interferometer (see Fig. 1). Again, reduced and enhanced correlations are observed. In contrast to Fig. 5 however, $R^{(\mathrm{n})}(s)$ is now a symmetric function of $s$, $R^{(\mathrm{n})}(-s)=R^{(\mathrm{n})}(s)$, because of the symmetry of the equipment.

For comparison, let us now consider disentangled two-photon states in the quantum regime or two uncorrelated classical pulses, i.e., light beams which are produced by independent sources. In this case in Eqs. (9) and (12), respectively, $K_1(s)$ [Eq. (11)] and $G_1(s)$ [Eq. (14)] read as

$$K_1(s)=\left|\int_0^\infty \mathrm{d}\Omega\,\alpha(\Omega)\int_0^\Omega \mathrm{d}\omega\,\omega\,|f(\omega)|^2\,e^{2i\omega s/c}T_{21}^{(\mathrm{I})^*}(\omega)T_{21}^{(\mathrm{II})}(\omega)\right|^2 \tag{19}$$

and

$$G_1(s)=2\left|\left\langle\int_0^\infty \mathrm{d}\omega\omega\,e^{2i\omega s/c}|f(\omega)|^2|T_{21}^{(\mathrm{I})^*}(\omega)T_{21}^{(\mathrm{II})}(\omega)\right\rangle\right|^2. \tag{20}$$

It is seen that the number of coincidence events can only be reduced, i.e., $R^{(\mathrm{n})}(s)\leq 1$, but not enhanced, $R^{(\mathrm{n})}(s)\not>1$.

Enhanced coincidences (as shown in Figs. 4 – 6) can therefore be regarded as being a signature of correlated beams. However it also depends on the band-shape functions of the interfering wave packets, whether enhanced coincidences can be observed or not. To be more specific, let us consider the band-shape functions $f^{(\mathrm{I/II})}(\omega)=T_{21}^{(\mathrm{I/II})}(\omega)f(\omega)$ of the wave packets in the two input ports of the beam splitter. The wave packets $f^{(\mathrm{I/II})}(\omega)$ will be said to be of type A if the Fourier transform

$$F(4s)=\int_{-\infty}^{\infty}\mathrm{d}\omega\,\left\{e^{4is\omega/c}\left[\Theta\Big(\omega+\tfrac{1}{2}\Omega\Big)-\Theta\Big(\omega-\tfrac{1}{2}\Omega\Big)\right]\right.$$

$$\times \left(\tfrac{1}{4}\Omega^2 - \omega^2\right) f^{(\mathrm{I})}(\omega) \left(f^{(\mathrm{II})}(\omega)\right)^* f^{(\mathrm{II})}(-\omega) \left(f^{(\mathrm{I})}(-\omega)\right)^* \Big\} \quad (21)$$

attains non-negative values only. Otherwise, the wave packets will be said to be of type B. In particular, it is easily seen that when $|f(\omega)|$ is a Gaussian and $T_{21}^{(\mathrm{I/II})}(\omega) = 1$, then $f^{(\mathrm{I/II})}(\omega)$ are of type A, whereas in the presence of a Bragg mirror, $T_{21}^{(\mathrm{I/II})}(\omega) \neq 1$, wave packets of type B can be produced. Recalling Eqs. (11) and (17), we find that for wave packets of type A the effect of enhanced coincidences cannot be observed on principle.

## 4 Summary and conclusions

We have studied the influence of wave-packet distortion at multilayer dielectric barriers on the coincidence-event output statistics in two-beam interference experiments of the type described in [8]. Usually the observed dependence of the interference fringes on the optical-path difference in the interferometer indicates that the wave packets prefer to arrive at equal output ports rather than different ones which in a sense can be interpreted as a "bunching" behaviour. However, when correlated wave packets are sufficiently distorted,

| | **Uncorrelated beams** | **Correlated beams** | |
|---|---|---|---|
| **Band shape** | Type A or B | Type A | Type B |
| **Classical beams** | $R^{(\mathrm{n})}(s) \leq 1$<br>$\mathcal{V} \leq \frac{1}{3}$ | | $R^{(\mathrm{n})}(s) \leq 1$<br>$R^{(\mathrm{n})}(s) > 1$<br>$\mathcal{V} \leq \frac{1}{2}$ |
| **Single-photon quantum beams** | $R^{(\mathrm{n})}(s) \leq 1$<br>$\mathcal{V} \leq 1$ | | $R^{(\mathrm{n})}(s) \leq 1$<br>$R^{(\mathrm{n})}(s) > 1$<br>$\mathcal{V} \leq 1$ |

Table 1
Conditions of reduction and enhancement of the number of coincidence events in the two output ports of the beam splitter in the Mach–Zehnder interferometer in Fig. 1.

then the opposite effect can also be observed, i.e., different output ports are preferably used and hence the number of coincidence events is enhanced, in correspondence to an "antibunching" behaviour of the wave packets at the beam splitter. The conditions under which the number of coincidence events is reduced or enhanced are summarized in Table 1, with special emphasis on the differences between quantum and classical light.

It should be noted out that similar effects are expected to be observed when the distortion of the wave packets is caused by other than multilayer devices. Finally, it should be pointed out that the diminished fringe visibility of the interference fringes in the classical regime has been derived for pulses produced in a random way, in close similarity to the quantum description of the down-conversion process. If there is an appropriate correlation between consecutive wave packet pairs, this visibility may be enhanced up to 100% also in the classical situation [16].

## References


[1] R. Gosh, C.K. Hong, Z.Y. Ou and L. Mandel, Phys. Rev. A 34 (1986) 3962.

[2] R. Gosh and L. Mandel, Phys. Rev. Lett. 59 (1987) 1903.

[3] H. Fearn and R. Loudon, J. Opt. Soc. Am. B 6 (1989) 917.

[4] R.A. Campos, B.E.A. Saleh and M.C. Teich, Phys. Rev. A 42 (1990) 4127.

[5] J.H. Shapiro and K.-X. Sun, J. Opt. Soc. Am. B 11 (1994) 1130.

[6] Y.H. Shih and A.V. Sergienko, Phys. Lett. A 186 (1994) 29.

[7] G. Weihs, M.Reck, H. Weinfurter and A. Zeilinger, Phys. Rev. A 54 (1996) 893.

[8] R.Y. Chiao, P.G. Kwiat and A.M. Steinberg, Quant. Semiclass. Opt. 7 (1995) 259; A.M. Steinberg and R.Y. Chiao, Phys. Rev. A 51 (1995) 3525.

[9] Ch. Spielmann, R. Szipöcs, A. Stingl and F. Krausz, Phys. Rev. Lett. 73 (1994) 2308.

[10] T. Gruner and D.–G. Welsch, Opt. Commun. 134 (1997) 447.

[11] M.V. Chekhova, S.P. Kulik, A.N. Penin and P.A. Prudkovsky, Opt. Commun. 132 (1996) 15.

[12] T. Gruner and D.–G. Welsch, in *Proceedings of the Third Workshop on Quantum Field Theory under the Influence of External Conditions*, Leipzig, 1995 (ed. M. Bordag, B.G. Teubner Verlagsgesellschaft, Stuttgart, Leipzig, 1996); Phys. Rev A 53 (1996) 1818.

[13] R. Matloob, R. Loudon, S.M. Barnett and J. Jeffers, Phys. Rev. A 52 (1995) 4823.

[14] T. Gruner and D.–G. Welsch, Phys. Rev A 54 (1996) 1661.

[15] J.M. Bendickson, J.P. Dowling and M. Scalora, Phys. Rev. E 53 (1996) 4107.

[16] T. Gruner, Ph.D. thesis, Friedrich-Schiller University of Jena, 1997.

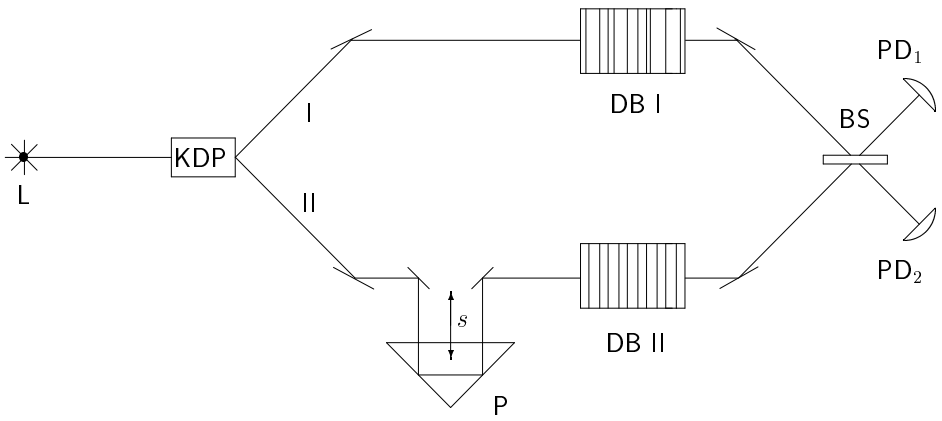


Figure 1: Scheme of an extended two-photon interference experiment of the type [8] for determining photon traversal times through multilayer dielectric barriers (L, laser; P, prism; DB I/II, dielectric barriers; BS, beam splitter; $PD_1$, $PD_2$, photodetectors).

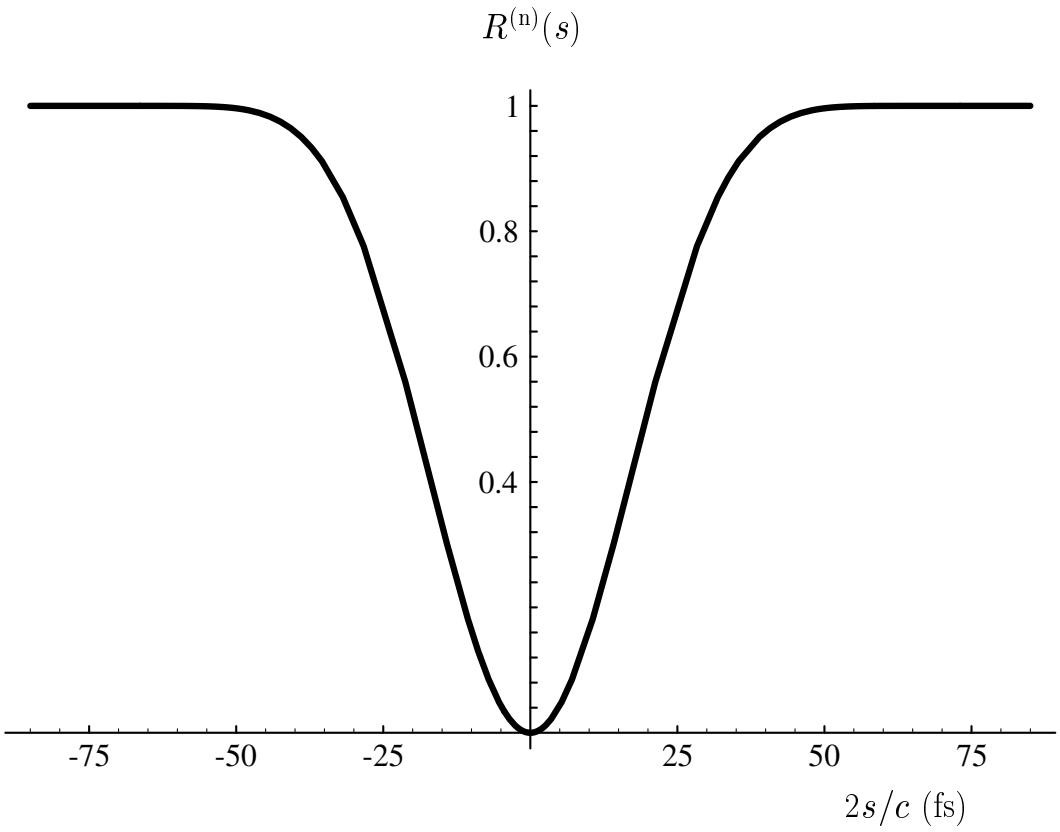


Figure 2: The (normalized) coincidences $R^{(\mathrm{n})}(s)$ are shown for an experimental scheme as shown in Fig. 1 in dependence on the translation length $s$ for time-limited pulses ($2t_0 = 40\,\mathrm{fs}$) of photons traveling in free space.

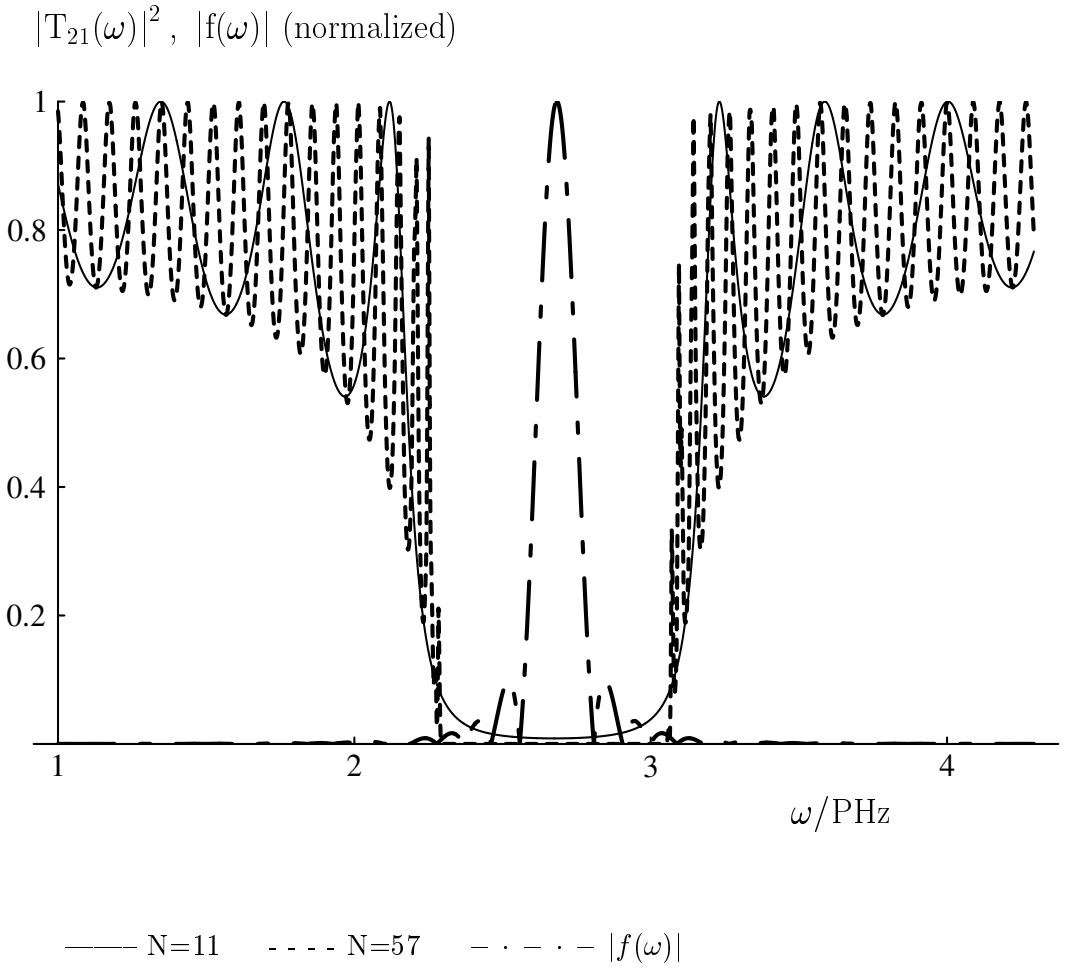


Figure 3: The square of the absolute value of the transmittance of a multilayer non-absorbing barrier ($n_{\mathrm{TiO_2}} = 2.22$, $n_{\mathrm{SiO_2}} = 1.41$), $|T_{21}(\omega)|^2$, is shown for $N = 11$ layers and $N = 57$ layers together with the (normalized) spectral line shape function of a pulse that is assumed to be limited in time ($2t_0 = 40\,\mathrm{fs}$).

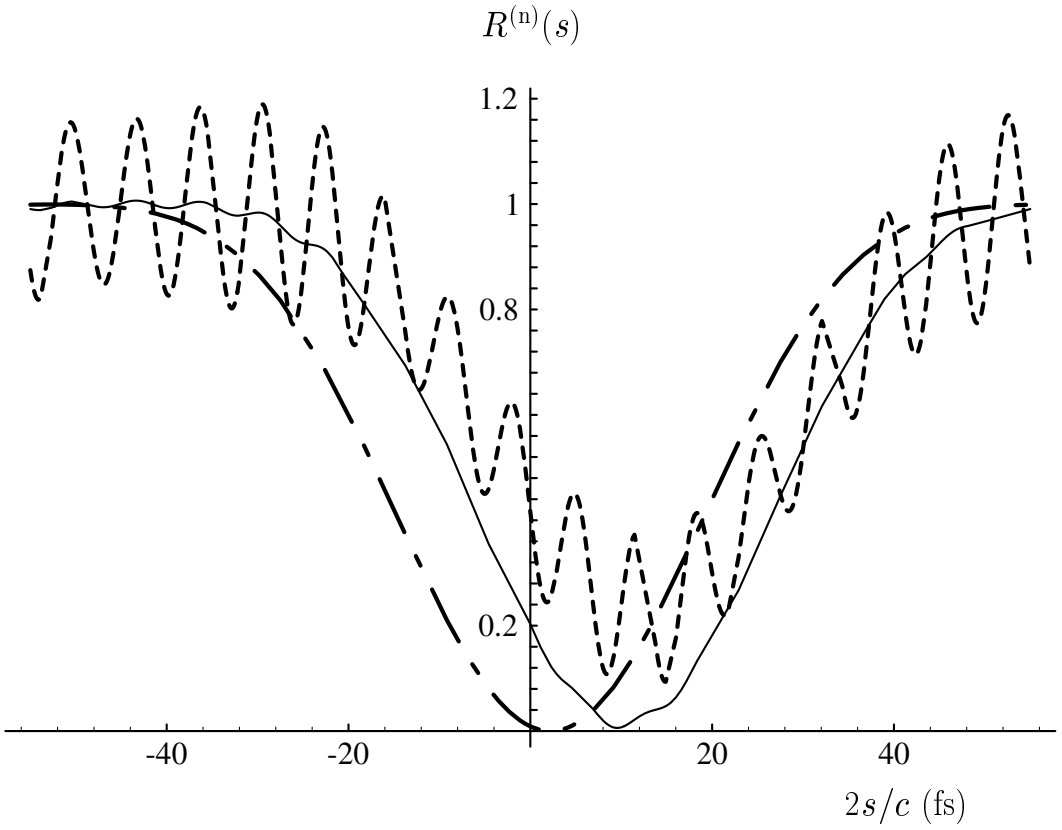


Figure 4: The (normalized) coincidences $R^{(\mathrm{n})}(s)$ are shown for an experimental scheme [8] in dependence on the translation length $s$ for a time-limited pulse of the incoming photon ($2t_0 = 40\,\mathrm{fs}$) and various numbers of the layers of a lossless barrier: $N = 11$ (dotted-dashed line), $N = 35$ (full line), $N = 41$ (dashed line). The data of the lossless barrier are the same as in Fig. 3.

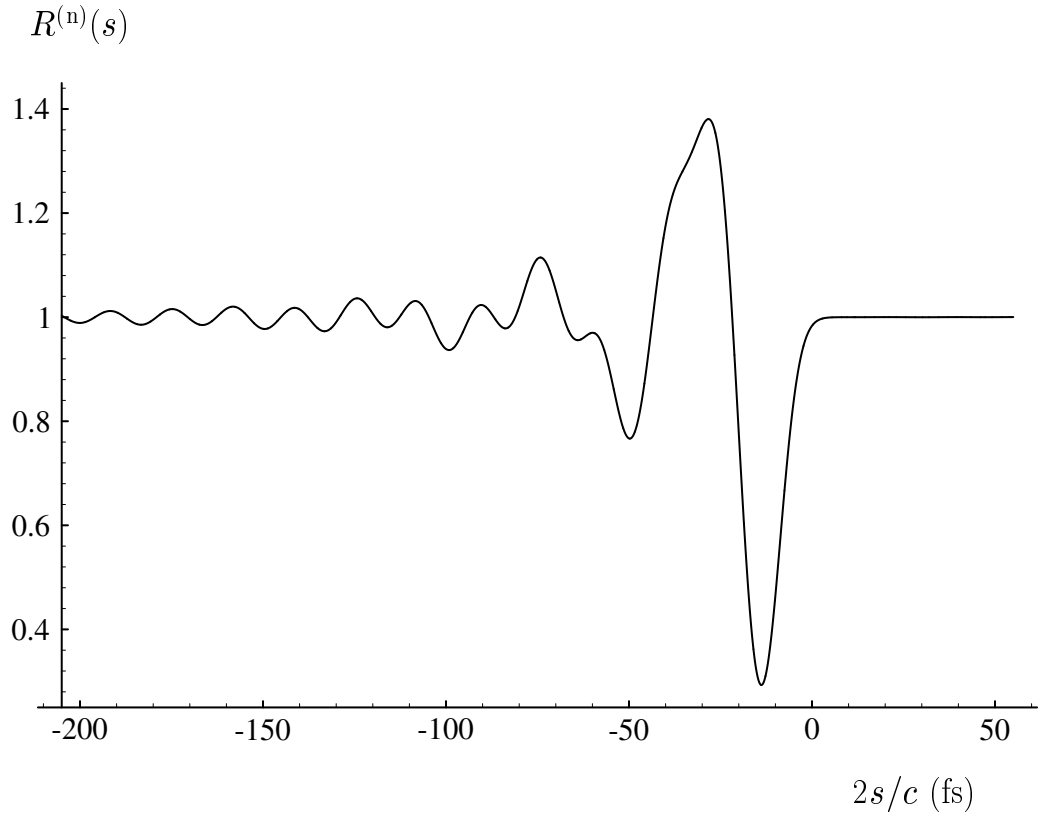


Figure 5: The (normalized) coincidences $R^{(\mathrm{n})}(s)$ are shown for an experimental scheme similar to [8] but for a laser frequency $\Omega = 6.22$ PHz, in dependence on the translation length $s$ for a time-limited pulse of the incoming photon ($2t_0 = 40\,\mathrm{fs}$) and a Bragg mirror with $N = 57$ layers. The data of the lossless barrier are the same as in Fig. 3.

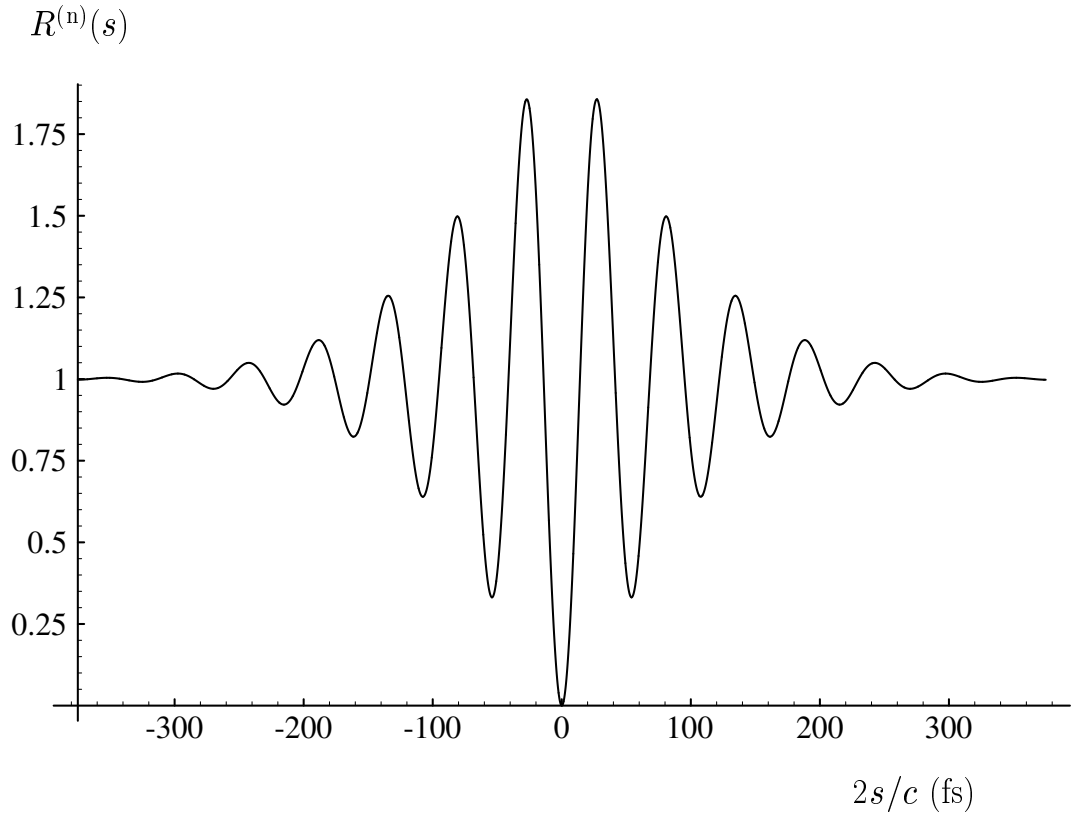


Figure 6: The (normalized) coincidences $R^{(\mathrm{n})}(s)$ in dependence on the translation length $s$ are shown for the experimental scheme sketched in Fig. 1 including two identical Bragg mirrors with $N = 57$ layers in path I and II. A laser frequency tuned to $\Omega = 6.16$ PHz and time-limited pulses of the incoming photons ($2t_0 = 40\,\mathrm{fs}$) have been assumed. The data of the lossless barriers are the same as in Fig. 3.